Contribution from the Department of Chemistry,
University of California, Berkeley, California 94720

Synthesis of *N*-Alkyl-3-hydroxy-2(1*H*)-pyridinones and Coordination Complexes with Iron(III)[1]

Robert C. Scarrow and Kenneth N. Raymond*

Received October 15, 1987

The amidation of 2,5-dimethoxytetrahydrofuran-2-carboxylic acid methyl ester by primary alkylamines followed by acid-catalyzed rearrangements yields *N*-alkyl-3-hydroxy-2-pyridinones. The rearrangement reaction is promoted by the presence of metal ions, such as Fe^{3+}, Cu^{2+}, and Zn^{2+}, which have high affinities for the bidentate hydroxypyridinone binding group. The structures of *N*-butyl-3-hydroxy-2-pyridinone (HL') and its 3:1 complex with iron(III) ($FeL'_3 \cdot 3H_2O$) have been determined by X-ray crystallography. Bond lengths involving the pyridine ring indicate that a catechol-like aromatic resonance form is significant, particularly in the iron complex. The visible spectra for $[FeL'_n]^{(3-n)+}$ (n = 1-3) are virtually identical with those of previously characterized complexes of iron(III) and 3-hydroxy-2(1*H*)-pyridinone (3,2-Hopo, HL). The log K_a (protonation constant) of HL' and log K_3 for formation of FeL'_3 (from $[FeL'_2]^+$ and $[L']^-$) are higher by 0.5 log unit than those of the unsubstituted HL and FeL_3. Differences in equilibria at pH >7 between solutions of FeL'_3 and those of FeL_3 have been studied by spectrophotometric titrations. The *N*-butyl derivative FeL'_3 hydrolyzes only above pH 10.5 in the presence of 3 mM excess HL', whereas three stepwise protonations (log K_a = 9.2, 10.6, 12) are observed in solutions of FeL_3 containing excess (several millimolar) HL. The contrasting behaviors of FeL'_3 and FeL_3 in alkaline solution are rationalized in terms of the absence or presence of a weakly acidic proton on the ligand nitrogens.

Introduction

A major goal of our research for the past several years has been the development of nontoxic and effective chelating agents for ions with high charge to ionic radius ratios.[2] One use of such ligands is chelation therapy for removal from the body of excess iron resulting from repeated blood transfusions employed in the treatment of certain anemias; oral iron poisoning, especially of infants, also is treatable by chelation therapy.[3,4] Many of the actinides (in particular, plutonium and thorium) exist in the tetravalent state in aqueous solution and show ligation preferences similar to that of trivalent iron; thus, chelation therapy for victims of plutonium contamination employs ligands similar to those for iron-removal therapy.[5] Other possible uses of this class of compounds are as aids in lowering background counts in tumor imaging employing radionuclides of gallium and indium[6] and as paramagnetic image-enhancement agents for whole-body magnetic resonance imaging.

We[1,2,7,8] and others[4,9] have prepared (catecholato)iron sequestering agents for iron(III) modeled after enterobactin, a catecholate-containing siderophore (microbial iron transport agent).[10,11] These ligands are produced by microbes to chelate extracellular iron and provide a biological model for synthetic ligands with both high affinity and high selectivity for ferric ion, as required for chelation therapy for iron overload.[3,4] Furthermore, since the iron transport function of the siderophores makes many of them potent growth factors for pathogenic bacteria, features associated with the specific recognition of such compounds and their transport should be avoided in the design of iron-chelating drugs.

Enterobactin is the siderophore with highest affinity for Fe^{3+} at neutral or higher pH.[10] However, the effectiveness at low pH of tricatechol enterobactin analogues is limited by their weak acidity and loss of six protons on binding iron(III). The hydroxypyridonates (whose anions are isoelectronic with catecholate dianions) and hydroxamates are stronger, monoprotic acids. Both are found in siderophores.[10] These ligands need only lose three protons to form six-coordinate bidentate complexes, which makes them competitive for iron at pH 7 with similar catecholate ligands, despite the much lower formation constants of the iron complexes. Indeed, the simple bidentate hydroxypyridinones 1,2-Hopo, 3,2-Hopo, and 3,4-Hopo (where "*x*,*y*-Hopo" is *x*-hydroxy-*y*(1*H*)-pyridinone) bind iron more completely than either catechol or acetohydroxamic acid under standard conditions at pH 7.[12] Although hydroxypyridinones have been shown to bind effectively to divalent transition metals,[13,14] the selectivity of bidentate hydroxypyridinones toward iron(III) over that toward divalent metals such as copper and zinc is comparable to that of catechol and better than that of hydroxamates.[12]

Bidentate hydroxypyridinones are produced by several microorganisms and presumed to be siderophores.[10] Similar ligands are promising agents for therapeutic removal of iron(III). The kinetic ability of 1,2-Hopo and 3,4-Hopo derivatives to remove iron from transferrin has been reported by Kontoghiorghes.[15,16] We have presented quantitative kinetic data which show that mimosine (a natural product amino acid derivative of 3,4-Hopo) and 3,4-Hopo remove iron in vitro from human iron transferrin at rates similar to those for tricatecholate ligands at concentrations as low as 2×10^{-4} M.[17] Some new synthetic hydroxypyridonate ligands show promising in vivo removal of plutonium in test animals.[18]

Previously we have shown that the tris(hydroxypyridonato)-iron(III) complexes of 1,2-Hopo and 3,2-Hopo are structurally similar to the tris(catecholato)ferrate trianion.[12,19] However,

* To whom correspondence should be addressed.

(1) Ferric Ion Sequestering Agents. 19. Part 18: ref 27.
(2) Raymond, K. N. In *Environmental Inorganic Chemistry*; Irgolic, K. J., Martell, A. E., Eds.; VCH: Deerfield Beach, FL, 1985; pp 331-347.
(3) May, P. M.; Bulman, R. A. *Prog. Med. Chem.* **1983**, *20*, 225-336.
(4) *Development of Iron Chelators for Clinical Use*; Martell, A. E., Anderson, W. F., Badman, D. G., Eds.; Elsevier/North Holland: Amsterdam, 1981.
(5) Raymond, K. N.; Kappel, M. J.; Pecoraro, V. L.; Harris, W. J.; Carrano, C. J.; Weitl, F. L.; Durbin, P. W. In *Actinides in Perspective*; Edelstein, N. M., Ed.; Pergamon: Oxford, England, and New York, 1982; pp 491-507.
(6) Moerlein, S. M.; Welch, M. J.; Raymond, K. N. *J. Nucl. Med.* **1982**, *23*, 501-506.
(7) Raymond, K. N.; Chung, T. D. Y.; Pecoraro, V. L.; Carrano, C. J. In *The Biochemistry and Physiology of Iron*; Saltman, P., Hegenauer, J., Eds.; Elsevier Biomedical: New York, 1982; pp 649-662.
(8) Raymond, K. N.; Pecoraro, V. L.; Weitl, F. L. In ref 4, pp 165-187.
(9) Kiggen, W.; Vögtle, F. *Angew. Chem., Int. Ed. Engl.* **1984**, *23*, 714-715.
(10) Raymond, K. N.; Müller, G.; Matzanke, B. F. In *Topics in Current Chemistry*; Boschke, F. L., Ed.; Springer: Berlin, 1984; Vol. 123, pp 49-102.
(11) Neilands, J. B. *Annu. Rev. Microbiol.* **1982**, *36*, 285-309.
(12) Scarrow, R. C.; Riley, P. E.; Abu-Dari, K.; White, D. L.; Raymond, K. N. *Inorg. Chem.* **1985**, *24*, 954-967.
(13) Stünzi, H.; Perrin, D. D.; Teitei, T.; Harris, R. L. N. *Aust. J. Chem.* **1979**, *32*, 21-30.
(14) Stünzi, H.; Harris, R. L. N.; Perrin, D. D.; Teitei, T. *Aust. J. Chem.* **1980**, *33*, 2207-2220.
(15) Kontoghiorghes, G. J. *Lancet* **1985**, *1*, 817.
(16) Taylor, D. M.; Kontoghiorghes, G. J. *Inorg. Chim. Acta* **1986**, *125*, L35. Kontoghiorghes, G. J.; Sheppard, L.; Barr, J. *Inorg. Chim. Acta* **1988**, *152*, 195-199.
(17) (a) Scarrow, R. C. Ph.D. Thesis, University of California, Berkeley, CA, 1985. (b) Kretchmar, S. A.; Craig, A.; Raymond, K. N., manuscript in preparation.
(18) White, D. L.; Durbin, P. W.; Jeung, N.; Raymond, K. N. *J. Med. Chem.* **1988**, *31*, 11-18.
(19) Scarrow, R. C.; White, D. L.; Raymond, K. N. *J. Am. Chem. Soc.* **1985**, *107*, 6540-6546.

0020-1669/88/1327-4140$01.50/0 © 1988 American Chemical Society

structural disorder prevented the accurate determination of bond lengths and angles. In this paper we report a synthetic method for *N*-alkyl derivatives of 3,2-Hopo. We report a pair of crystal structures that show the importance of the localized and aromatic resonance structures in both the free ligand and the complex with iron(III). The complexes formed between *N*-butyl-3-hydroxy-2(1*H*)-pyridinone (HL′) and iron(III) in neutral or acidic solution have similar stabilities and are spectroscopically similar to the complexes of 3,2-Hopo (HL) and ferric ion. However, spectrophotometric titration results indicate FeL_3 deprotonates above pH 8, whereas the alkylated derivative (FeL'_3) is stable to hydrolysis or deprotonation to above pH 10.

Experimental Section

Chemicals were purchased as follows: methyl 2-furoate, butylamine, and chloroform-*d* from Aldrich, 50:50 nickel/aluminum alloy (from Raney Nickel) from Alfa, ferric perchlorate from G. F. Smith, and other metal salts from Mallinckrodt. Organic solvents and mineral acids were of reagent grade and were used as supplied. Butylamine and diethyl ether were distilled before use. Concentration of Fe^{3+} in the ferric perchlorate stock solution was determined by titration with ethylenediaminetetraacetic acid.[12]

Elemental analyses and NMR spectra were obtained at facilities of the Department of Chemistry, University of California, Berkeley, CA. The reported ^1H NMR spectra were obtained in $CDCl_3$ containing ca. 1% tetramethylsilane as reference by using a Nicolet 200 MHz spectrophotometer. Infrared spectra were taken between KBr plates by using a Perkin-Elmer Model 293 spectrometer.

2,5-Dimethoxytetrahydrofuran-2-carboxylic Acid Methyl Ester (1). Electrolytic oxidation of methyl 2-furoate in methanol gives 2,5-dimethoxy-2,5-dihydrofuran-2-carboxylic acid methyl ester.[20] The latter was hydrogenated by using a modification of the literature procedure:[20] 35.2 g of the dihydrofuran in 200 mL of methanol containing 2–3 g of Raney Nickel W-2[21] was stirred at room temperature in a Parr reactor for 22 h under 700–800 psi of H_2. The NMR spectrum showed the hydrogenation to be complete with diastereomers present in a 55:45 ratio, with methyl singlets at 3.817, 3.48, 3.37 (major isomer), 3.812, 3.43, and 3.31 ppm (minor isomer). Also observed were multiplets at 5.24 (assigned to 5-H) and 1.9–2.4 ppm. The product was vacuum-distilled (35 °C at ca. 0.02 Torr) and 29.6 g (83%) of distillate of **1** collected. Anal. Calcd (found) for $C_8H_{14}O_5$: C, 50.52 (50.66); H, 7.42 (7.37).

***N*-Butyl-2,5-dimethoxytetrahydrofuran-2-carboxamide (2).** An equimolar solution of 1.02 g (5.4 mmol) of **1** and 0.40 g of freshly distilled *n*-butylamine was heated at reflux for 6 h, after which an NMR spectrum of an aliquot showed a 3:1 ratio of **1** to **2**. Thus, the reaction was run in an excess of amine: 2.2 g of *n*-butylamine was added and the solution refluxed for 7 h. The reaction mixture was rotary-evaporated at room temperature to yield **2** (0.94 g, 76%). Anal. Calcd (found) for $C_{11}H_{21}NO_4$: C, 57.12 (57.15); H, 9.15 (9.32); N, 6.06 (6.22). Doubling of amide and one of the methyl NMR resonances (6.89, 6.82 and 3.34, 3.28 ppm) at −45 °C indicates two isomers are present. Other NMR resonances are at 5.30 (5-H), 3.52 (methyl), 1.9–2.4 (3-H and 4-H), and 3.37, 1.56, 1.39, and 0.95 ppm (butyl group). The IR spectrum of **2** shows amide ν = 1675 cm^{-1}. A 1% impurity of **1** was detected by both NMR and IR spectroscopies (ν_{CO} for **1** = 1750 cm^{-1}).

Tris[*N*-butyl-3-hydroxy-2(1*H*)-pyridinonato]iron(III) Trihydrate (4; $FeL'_3 \cdot 3H_2O$). A solution containing 0.128 g (0.55 mmol) of **2**, 0.19 mmol of $Fe(ClO_4)_3$, and 0.34 mmol of $HClO_4$ in a total volume of 2.8 mL was deoxygenated and left at room temperature under argon for 10 days. A dark purple solid formed on the sides of the reaction vessel. This was dissolved in water, and the solution was extracted with 12 mL of 3:1 chloroform/pyridine. The organic phase was washed once with 8 mL of aqueous 4 M sodium chloride and once with 10 mL of water. The organic solvent was removed by rotary evaporation to leave a purplish glassy coating on the sides of the flask (0.11 g = 0.18 mmol; ca. 95% based on **2**). This was crystallized by dissolving the solid in 5 mL of methanol and 10 mL of water and slowly evaporating the solution. The crystal used for X-ray data collection was obtained by slow cooling of a boiled and filtered aqueous solution of FeL'_3.

The water of crystallization was removed by drying in vacuo (ca. 0.02 Torr) at 75 °C for 45 min. Anal. Calcd (found) for $C_{27}H_{36}FeN_3O_6$: C, 58.49 (58.45); H, 6.54 (6.54); N, 7.58 (7.61).

***N*-Butyl-3-hydroxy-2(1*H*)-pyridinone (3; HL′).** A solution of 0.22 g (0.95 mmol) of **2** in 1.0 mL of aqueous 0.1 M HNO_3 was deoxygenated by three freeze–pump–thaw cycles and maintained under argon gas while being refluxed at 115 °C for 2 h. This produced both white crystals (presumed HL′) and a brown oil (presumed decomposition product). Both the crystals and oil dissolved in 5 mL of dichloromethane/heptane (3:2) added to the reaction flask. The aqueous layer was further extracted with three 3-mL portions of CH_2Cl_2 and then with 3 mL of heptane. The nonaqueous washings were combined and evaporated, and then the residue was redissolved in 5 mL of heptane and 1 mL of CH_2Cl_2. Treatment with one 6-mL portion followed by five 3 mL-portions of aqueous ammonia (1 M) resulted in preferential extraction of HL′, leaving a brown nonaqueous layer. The aqueous layer was rotary-evaporated to dryness, the residue redissolved in 6 mL of water and 4 mL of methanol, and the solution rotary-evaporated to near dryness. Removal of the remaining solvent followed by vacuum-drying at ca. 50 °C gave 0.119 g (75%) of very slightly brownish HL′. Anal. Calcd (found) for $C_9H_{13}NO_2$: C, 64.65 (64.42); H, 7.84 (7.95); N, 8.38 (8.27).

Alternately, HL′ could be prepared by digestion of $FeL'_3 \cdot 3H_2O$, albeit in poor yield (ca. 10%). For instance, $FeL'_3 \cdot 3H_2O$ was heated in 2 M aqueous NaOH and the solution filtered to remove ferric hydroxide precipitate. The filtrate was neutralized with hydrochloric acid and extracted into dichloromethane, and the solution was then removed by rotary evaporation to leave a dark red solid. The ligand was preferentially dissolved in hot hexane, and the solution was filtered and allowed to cool and slowly evaporate. Large clear single crystals of HL′ resulted; an oily coating was removed from the crystals by rubbing them with damp paper tissues. Anal. Found: C, 64.84; H, 7.85; N, 8.38. One of these crystals was used for collecting X-ray diffraction data.

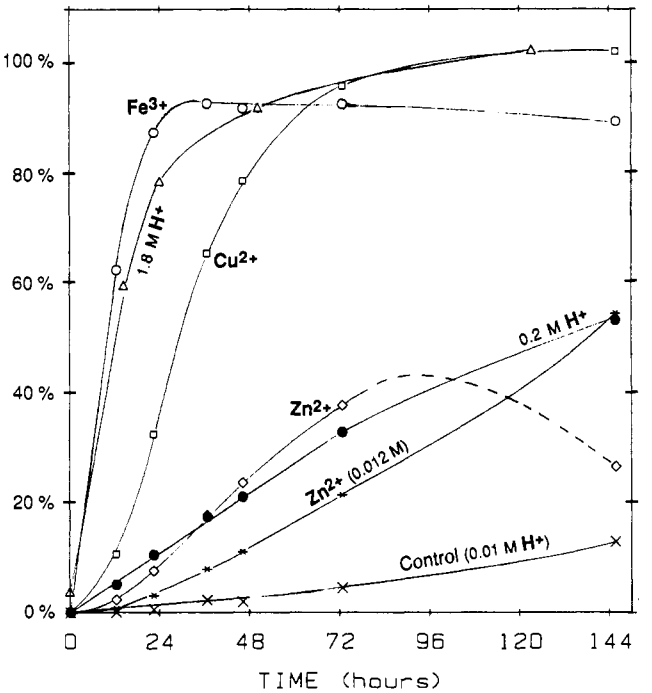

Figure 1. Kinetics of the transformation of **2** to HL′, monitored as described in the Experimental Section. The initial concentration of **2** was 0.12 M (0.105 M for the reaction in 1.8 M HNO_3). The control and metal ion reactions were 0.01 M in nitric acid. Reactions with metal ions contained 0.12 M metal salt, except as indicated for one of the Zn^{2+} reactions.

Kinetics of Transformation of 2 to HL′. A deoxygenated solution 0.117 M in **2** and 0.01 M in HNO_3 was measured into vials, which were kept under argon. Concentrated nitric acid or metal salts ($FeCl_3 \cdot 6H_2O$, $Cu(NO_3)_2 \cdot 3H_2O$, $ZnSO_4 \cdot 7H_2O$) were added to give the solutions described in Figure 1.

The reaction progress was monitored by observation of the blue color of $[FeL']^{2+}$. Like $[FeL]^{2+}$ (HL = 3,2-Hopo), this complex has λ_{max} = 600 nm.[12] An aliquot (0.018 mL; Eppendorf pipets) was removed periodically from one of the seven reaction solutions and added to 3.0 mL of a solution 0.0035 M in $Fe(ClO_4)_3$ and 0.01 M in HNO_3. The absorbance at 600 nm was measured in 1-cm quartz cuvettes on a Cary 117 spectrophotometer within 1 or 2 min of mixing the assay solution. The extent of reaction was calculated by assuming ϵ = 1810 M^{-1} cm^{-1}.[12]

X-ray Crystallography. Diffraction-quality crystals of HL′ and $FeL'_3 \cdot 3H_2O$ were obtained as described above and were mounted with epoxy on the end of a glass fiber. Crystals were evaluated for diffraction quality on the basis of Laue and precession photographs, and the space group was determined by the automatic search routine of the Enraf-

(20) Clauson-Kaas, N.; Limborg, F. *Acta Chem. Scand.* **1952**, *6*, 551–555.
(21) Mozingo, R. *Organic Syntheses*; Wiley: New York, 1955; Collect. Vol. III, pp 181–183.

Table I. Crystallographic Summary (Estimated Standard Deviations in Parentheses)

	HL′	$FeL'_3 \cdot 3H_2O$
mol formula	$C_9H_{13}NO_2$	$C_{27}H_{42}FeN_3O_9$
fw	167.21	608.5
$F(000)$, e	360	1938
space group	$P2_1/n^a$	$R\bar{3}$ (hex)
a, Å	8.016 (1)	14.937 (2)
b, Å	11.564 (1)	
c, Å	10.011 (1)	24.276 (2)
β, deg	99.38 (1)	
V, Å^3	915.5 (2)	4691 (1)
Z, formula units/cell	4	6
d_{calc}, g/cm^3	1.231	1.291
d_{obs}, g/cm^3	not determd	1.26[b]
data cryst shape	parallelepiped	irregular
data cryst size, mm	0.28 × 0.25 × 0.18	0.32 × 0.22 × 0.19
wavelength, Å (radiation)	0.71073 (Mo Kα)	0.71073 (Mo Kα)
2θ range, deg		
cell constants	27–29	27–28
data collcn	1–50	2–55
data collcn time, h	38	112
cryst decay[c]	28% (cor)	1% (uncor)
variation in intens, in azimuthal scans[d]	2%	4%
p factor for weighting[e]	0.02	0.02
no. of unique nonabsent reflcns measd	1607[f]	2401[g]
no. of obs reflcns,[h] n_o	810	1228
no. of refined params, n_v	113	133
extinction param	2.0 (4) × 10^{-6}	none included
resid, final structure[i,j]		
R	0.039	0.036
R_w	0.045	0.041
R_{all}	0.084	0.084
E	2.18	1.79
largest peak in final, diff Fourier, e/Å^3	0.15	0.27

[a] $P2_1/n$ is an alternate setting of space group $P2_1/c$ with equivalent positions $\pm(x, y, z)$, $\pm(^1/_2 - x, ^1/_2 + y, ^1/_2 - z)$. [b] The density of $FeL'_3 \cdot 3H_2O$ was determined by flotation in aqueous KI. [c] Three high-intensity reflections were checked every 2 h of data collection as a measure of crystal decay. The number given is the percent decline in the measured intensity of these intensity standards over the time of data collection. In the case of HL′ the data were corrected for decay by using the average intensity decline of the three intensity standards. [d] For each crystal, five intense reflections spanning the 2θ range were rotated about the diffraction vector in 10° increments; the average variation in intensity caused by this rotation is reported. No absorption correction was performed. [e] Weights were assigned by using a factor (p) to account for estimated error in addition to that from counting error in data collection. The p values were determined from the statistics of averaging equivalent reflections. [f] The total of 3127 measured reflections ($+h,\pm k,\pm l$; $0,\pm k,+l$; $0,\pm k,0$) included 1520 symmetry-related reflections that were averaged. [g] A total of 4800 reflections were measured, including 2399 Friedel pairs that were averaged. [h] Reflections with $F^2 > 3\sigma(F^2)$ were considered observed and were used in the least-squares refinement. [i] The function minimized in refinement is $D = \sum w(|F_o| - |F_c|)^2$; error indices are $R_w = (D/\sum wF_o^2)^{1/2}$, $R = (\sum||F_o| - |F_c||)/\sum|F_o|$, and $E = [D/(n_o - n_v)]^{1/2}$, where n_o = number of "observed" reflections (see footnote [h]), n_v = number of variables refined, and the sums are over observed reflections. [j] R_{all} is defined as R, but the sum is over all measured reflections.

Nonius CAD 4 diffractometer. Details of data collection and refinement are given in Table I.[22] The structure of HL′ was solved by direct methods using MULTAN,[23] and the structure of $FeL'_3 \cdot 3H_2O$, by standard heavy-atom techniques.[22]

Titration Studies. All titrations were carried out at 25 °C and with $\mu = 0.10$ maintained by KCl or KNO_3; equilibrium constants are reported in concentration rather than activity units. The p[H] (=−log [H$^+$]) was measured by using a Corning 130 pH meter and a TRIZMA (Sigma) combination electrode kept in the reaction vessel. The electrode was calibrated with dilute (ca. 0.004 M) standardized HNO_3 and KOH solutions adjusted to 0.10 M ionic strength with KNO_3.

UV–vis spectra were measured on a Hewlett-Packard 8450a diode-array spectrophotometer. Additions of titrant were normally made with a Sargeant-Welch automatic buret, although in some cases the additions were made manually by using calibrated 2.0-mL Gilmont pipets. Except in this latter case, the spectrophotometric titrations were controlled by a Commodore PET computer with 12-kbyte memory and an interface device constructed by the Electronics Shop of the Department of Chemistry, University of California, Berkeley, CA. The software for controlling this titration apparatus was written in PET BASIC. After each titrant addition, the reaction solution was cycled to and from the quartz cell several times to achieve thorough mixing.[24]

To ensure complete mixing and equilibration, spectra were measured at 1–2-min intervals after each titrant addition. The difference between successive spectra (the nth and $(n + 1)$th spectra) was quantified as RMS(ΔA), defined as

$$\mathrm{RMS}(\Delta A) = [[\sum(A_{n+1}(\lambda) - A_n(\lambda))^2]/n_\lambda]^{1/2}$$

where the sum is over all wavelengths measured in the spectral region of interest (the HP 8450a has a diode detector every 2 nm from 400–800 nm) and n_λ is the number of wavelengths. Back-to-back spectra of the initially prepared titration solution were used to estimate the magnitude of RMS(ΔA) that could be attributed to spectrophotometer noise, and this value (usually about 0.0005) was used to determine when equilibrium had been reached. The spectral changes observed appear to be complete within 1 or 2 min.

A series of six titrations of solutions 0.010–0.035 mM in total iron(III) and 2.8–12.6 mM in total 3,2-Hopo were performed. In addition, a titration of ligand only was performed to determine the contribution to the absorbance from the protonated and deprotonated 3,2-Hopo species. Solutions were prepared with 0.10 M KCl, and either 12 M HCl or 0.10 M KOH was used to adjust the p[H] within the range 4–12. This ensured constant 0.10 M ionic strength. The six titrations were performed over a period of 48 h by using the same stock solutions of iron and ligand (the latter was kept under argon to minimize oxidation).

The titrations were on an initial 40–50-mL volume of solution in a 10.0-cm quartz cell connected via a ground-glass joint to a water-jacketed (25 °C) reaction vessel. The reaction vessel was kept higher than the 10-cm cell, but the solution could be pumped back to the reaction vessel by using a positive pressure of argon applied through a second ground-glass opening in the cell. Water-saturated argon was passed over the top of the solution in the reaction vessel.

The potentiometric determination of the protonation constant (K_a) of HL′ was carried out under argon by using KOH as titrant. A spectrophotometric titration of a solution 0.037 mM in iron(III) and 3.1 mM in HL′ used KNO_3 as the supporting electrolyte. The titration (with 0.10 M KOH spanning p[H] 2.3–12.2) was performed under argon on 5.0 mL of solution in a 1.0-cm quartz cuvette. A 12-mm-i.d. quartz tube was attached to the top of the square cuvette to increase its capacity and to accommodate the electrode, buret tip, and an argon inlet used to aid in vertical mixing. The solution was magnetically stirred and maintained at 25 °C by a Hewlett-Packard 89100a temperature-controlled cuvette holder. Extinction coefficients for the UV tail of the ligand alone were calculated from the slight absorbance observed for ligand-only absorbance solutions and the potentiometrically determined log K_a.

Calculations from Spectrophotometric Titrations. Spectral componentization was used to determine the minimum number of absorbing species that must be used to accurately model the absorbance spectra.[25] This technique approximates each spectrum from a titration as a linear combination of a small number (n_c) of mutually orthogonal "component spectra", denoted $V_i(\lambda)$. Thus, the approximated spectrum, $A_{calc}(\lambda) = \sum x_i V_i(\lambda)$, where x_i is independent of λ. For a given set of spectra and fixed value of n_c, principal component analysis[26] determines the component spectra and a set of linear coefficients (x_i) for each spectrum. This is done so as to minimize the least-squares residual

$$||R|| = \left(\frac{\sum_{\text{spectra}} \sum_\lambda (A_{obs} - A_{calc})^2}{n_{\text{spectra}} n_\lambda} \right)^{1/2} \quad (1)$$

In order not to lose spectral information, n_c is chosen as the minimum value that reduces $||R||$ near the level of instrumental noise (0.0001–0.0005 absorbance unit, depending on the absorbance of the

(22) For additional details of data collection and processing, see: Eigenbrot, C. W.; Raymond, K. N. *Inorg. Chem.* **1982**, *21*, 2650.
(23) "Structure Determination Package User's Guide"; B. A. Frenz and Associates, Inc.: College Station, TX, 1982.
(24) Further details of the spectrophotometric titration apparatus may be found in: Loomis, L. Ph.D. Thesis, University of California, Berkeley, CA, 1986.
(25) Maeder, M.; Gampp, H. *Anal. Chim. Acta* **1980**, *122*, 303–313.
(26) Mardia, K. V.; Kent, J. T.; Bibby, J. M. *Multivariate Analysis*; Academic: London, 1979; Chapter 8.

Scheme I

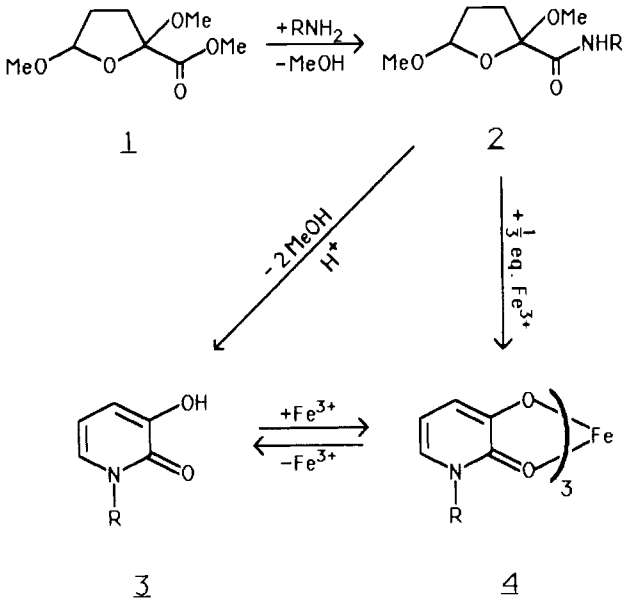

solution). This value of n_c is a minimum value for N_{comp} and usually equals N_{comp}, the number of absorbing species present during the titration. (If $N_{comp} > n_c$, then one such species would necessarily have an extinction coefficient spectrum that was very nearly a linear combination of those of the other species, which is unlikely.) In addition to indicating N_{comp}, spectral componentization describes each spectrum by n_c values of x_i, which may be used in place of absorbance values for all data treatments based on Beer's law.[25] Since 125 wavelengths (from 402 to 650 nm) have been used in our analyses, the n_c (=3, 4) component coefficients (x_i) represent a considerable reduction in data and enable subsequent analysis to be performed in a few minutes on a microcomputer. The FORTRAN program REFSPEC[17a,27] uses the x_i and V_i to evaluate various solution equilibria models for metal–ligand complexation. Given a model, REFSPEC determines the values of equilibrium constants and extinction coefficients that give the best least-squares fit to the data.

Results and Discussion

Synthesis. The general method for synthesis of N-substituted derivatives of 3,2-Hopo is as shown in Scheme I (the numbers identify the molecules, where R = *n*-butyl). In addition to the synthesis of the *N*-butyl derivative **3** (HL′), the *N*-ethyl- and *N*-propyl-3-hydroxy-2(1*H*)-pyridinones have been prepared by similar procedures.

The reaction of **1** with a primary amine in methanol occurs over days at room temperature. Addition of acetic acid was tried as a means of reducing the OH^- concentration in order to disfavor the formation of 2,5-dimethoxytetrahydrofuran-2-carboxylic acid; however, this slowed considerably the amidation reaction. The reaction of **1** with butylamine gave a good yield when run in excess refluxing butylamine for several hours. For higher molecular weight amines, such as might be used in the synthesis of molecules containing multiple hydroxypyridinone groups, a solvent would be desirable.

The transformation of the amide derivatives such as **2** into *N*-alkylhydroxypyridinones occurs when **2** is refluxed in 0.1–1.0 N mineral acid (HCl, HNO_3, and H_2SO_4 have all been used) for 1 or 2 h. Complicating the purification of **3** is the yellowish degradation product that forms during refluxing despite efforts to keep out oxygen. It was hypothesized that room-temperature reaction might diminish the formation of this yellow product. Thus, the kinetics of the transformation of **2** to **3** at room temperature were followed by the assay procedure described in the Experimental Section.

It was discovered that this reaction is accelerated both by protons and by transition-metal ions with high affinities for 3,2-Hopo (see Figure 1). The rate of acceleration parallels the binding affinity of the metals for 3,2-Hopo: $Fe^{3+} > Cu^{2+} > Zn^{2+}$.[12,14] The copper and zinc systems exhibit an induction period; this may be an indirect effect due to the release of protons as HL′ is formed and binds to the metal or may indicate that the active intermediate species is the metal–hydroxypyridinone complex. Figure 1 shows that, after 6 days at room temperature, two of the reactions were complete. These were the reaction in 1.8 M HNO_3 and the reaction containing 1 equiv of cupric nitrate and 0.01 M HNO_3. The apparent incompleteness of the Fe^{3+}-promoted reaction, despite its rapid start, was due to precipitation of $FeL'_3 \cdot 3H_2O$, since a small amount of purple solid was observed on the surface of the iron-containing solution on day 6.

Although the zinc(II)-catalyzed reaction was slower, it shows promise from a preparative standpoint. On the basis of the formation constant of ZnL^+,[14] the ZnL′ complex should not form in significant quantity at pH 2, which would ease recovery of the free ligand. In fact, analytically pure crystals of HL′ were found on day 6 in the reaction solution containing 1 equiv of $ZnSO_4$, which accounts for the observed decrease of product in solution (Figure 1).

Structure of *N*-Butyl-3-hydroxy-2(1*H*)-pyridinone (HL′). Large (up to 1 mm^3) clear parallelepiped crystals of HL′ were obtained by slow evaporation of a saturated hexane solution. One of the smaller of these was selected for measurement of X-ray diffraction, on the basis of sharp spots shown in Laue photographs. Crystal decay was significant over the course of data collection; correction was made for its effects by using the intensity standards. Measured properties of the crystal and details of data collection are given in Table I. The structure was solved by direct methods.[23] Refinement of all non-hydrogen positions and anisotropic thermal parameters allowed hydrogen atoms to be identified as 13 of the 14 highest peaks in the difference Fourier map. These were fixed at idealized positions (effective C–H distances of 0.95 Å[28] with isotropic thermal parameters (*B*'s) of 9 $Å^2$, except for the hydroxyl proton, the position of which was refined while the isotropic thermal parameter was fixed at 7 $Å^2$. The *R* values and other information pertaining to the final least-squares refinement are given in Table I.

The refined atomic coordinates and B_{eq}'s are given in Table II, and Table III gives selected bond lengths and angles. Tables S-1–S-3 give refined anisotropic thermal parameters, fixed hydrogen positions and thermal parameters and observed and calculated structure factors.[29]

Structure of Tris[*N*-butyl-3-hydroxy-2(1*H*)-pyridinonato]-iron(III) ($FeL'_3 \cdot 3H_2O$). The choice of $R\bar{3}$ as the space group was confirmed by the final structure. Note that the trihydrate formulation is based both on density determination and on successful location of water in the structure refinement. The dimensions

Table II. Final Positional Parameters and B_{eq}'s (Isotropic Equivalent Thermal Parameters) for *N*-Butyl-3-hydroxy-2(1*H*)-pyridinone (HL′)[a]

atom	*x*	*y*	*z*	B_{eq},[b] $Å^2$
O1	0.5415 (2)	0.3731 (1)	0.0518 (1)	6.10 (4)
O2	0.2323 (2)	0.4788 (1)	0.0255 (2)	6.45 (4)
N	0.4731 (3)	0.2530 (2)	0.2146 (2)	6.12 (5)
C1	0.4361 (3)	0.3407 (2)	0.1221 (2)	5.18 (5)
C2	0.2710 (3)	0.3903 (2)	0.1133 (2)	5.43 (5)
C3	0.1569 (3)	0.3488 (2)	0.1864 (2)	7.31 (6)
C4	0.2017 (4)	0.2573 (2)	0.2778 (3)	8.34 (7)
C5	0.3560 (4)	0.2118 (2)	0.2902 (2)	7.78 (7)
C6	0.6397 (4)	0.1991 (2)	0.2286 (3)	7.40 (7)
C7	0.6419 (4)	0.0987 (3)	0.1302 (2)	7.50 (7)
C8	0.8071 (4)	0.0431 (3)	0.1398 (3)	8.94 (9)
C9	0.8092 (4)	−0.0568 (3)	0.0430 (3)	8.93 (9)
H2	0.328 (3)	0.505 (2)	0.004 (2)	7.0*

[a] See Figure 2 for identity of the atoms; H2 is bonded to O2; numbers in parentheses are estimated standard deviations of the last digit. [b] Asterisk indicates a fixed isotropic thermal parameter.

(27) Turowski, P. T.; Rodgers, S. J.; Scarrow, R. C.; Raymond, K. N. *Inorg. Chem.* **1988**, *27*, 474–481.
(28) Churchill, M. R. *Inorg. Chem.* **1973**, *12*, 1213–1214.
(29) Supplementary material: see the paragraph at the end of this paper regarding content and order information.

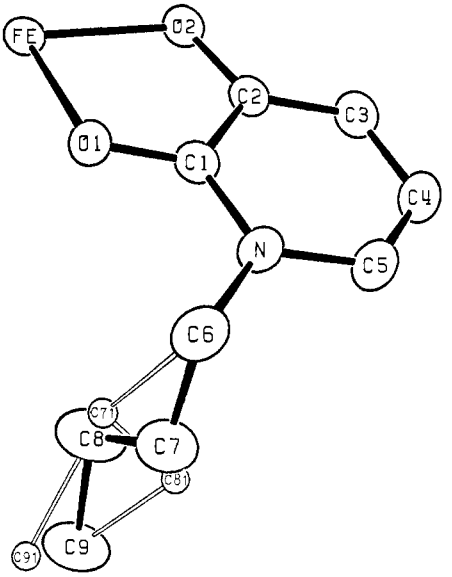

Figure 2. Atom-naming scheme and disorder model for $FeL'_3 \cdot 3H_2O$. Anisotropic atoms are shown at the 20% probability level. Isotropic partial (<0.5) occupancy carbon atoms are shown with arbitrary radii. In addition to the atoms shown, the water oxygen is named OW and hydrogen atoms are numbered in accordance with the atom to which they are bound. The water protons were not included in the model.

of the unit cell changed slightly over the course of data collection; *a* shrank by 0.05%, while *c* expanded by 0.03%, leaving the volume virtually unchanged. The small changes in the magnitude of intensity standards and the low *R* values obtained for the final structure indicate that this structural change was relatively minor.

The structure was solved by heavy-atom techniques. Refinement of an initial ordered model gave very large anisotropic thermal parameters for C7–C9, and a difference Fourier map showed alternate positions for each of these atoms. Various models of the disorder were tried and evaluated on the basis of their ability to match the electron density and give plausible bond lengths. The model chosen includes three alternate butyl group conformations as shown in Figure 2, which result in one major (modeled anisotropically) and one minor (modeled isotropically) position for each of the three carbon atoms C7–C9. Fractional occupancies of the three conformations were adjusted (by increments of 0.05) to give the best fit. Hydrogen atoms were added at idealized positions in the last stages of refinement to give the error indices of Table I; refined positional and B_{eq} parameters and anisotropic thermal parameters are given in Tables IV and S-4,[29] respectively. Fixed hydrogen positions, thermal parameters, and occupancy factors are in Table S-5, and structure factors are given in Table S-6.[29]

Table III. Bond Lengths (Å) and Angles (deg) Calculated for *N*-Butyl-3-hydroxy-2(1*H*)-pyridinone (HL'), Its Iron Complex (FeL'_3), and FeL_3[21] [a]

	HL'	FeL'_3	FeL_3
	Distances		
C1–O1	1.242 (2)	1.268 (2)	1.25 (1)
C2–O2	1.352 (2)	1.323 (2)	1.37 (1)
C1–C2	1.432 (2)	1.435 (3)	1.439 (4)
C2–C3	1.349 (2)	1.366 (3)	1.42 (1)
C3–C4	1.406 (3)	1.404 (4)	1.397 (5)
C4–C5	1.331 (3)	1.333 (3)	1.358 (7)
C5–N	1.383 (3)	1.365 (3)	1.350 (5)
N–C1	1.373 (2)	1.357 (3)	1.30 (1)
N–C6	1.460 (3)	1.470 (3)	
C6–C7	1.525 (3)	1.445 (5)	
C7–C8	1.461 (3)	1.422 (7)	
C8–C9	1.510 (3)	1.592 (9)	
O1–H2(Fe)	1.897 (18)	2.049 (1)	2.016
O2–H2(Fe)	0.880 (18)	1.980 (1)	2.016
O2–OW		2.740 (2)	
OW–OW		2.612 (3)	
	Angles		
O1–C1–C2	123.5 (2)	119.5 (2)	
O2–C2–C1	117.0 (2)	114.2 (2)	
N–C1–C2	115.7 (2)	119.0 (2)	123.4 (9)
C1–C2–C3	121.7 (2)	118.7 (2)	113.6 (8)
C2–C3–C4	119.8 (2)	119.5 (2)	121.4 (6)
C3–C4–C5	119.6 (2)	121.0 (2)	119.1 (4)
C4–C5–N	121.1 (2)	120.5 (2)	120.9 (4)
C5–N–C1	122.1 (2)	121.3 (2)	121.6 (6)
C1–N–C6	118.3 (2)	118.3 (2)	
N–C6–C7	111.7 (2)	113.5 (3)	
C6–C7–C8	113.4 (2)	118.0 (5)	
C7–C8–C9	113.5 (2)	115.7 (5)	
O1–Fe–O2		80.51 (6)	80.85 (5)
C1–O1–Fe		110.7 (1)	
C2–O2–H2(Fe)	107.4 (12)	113.9 (1)	
trigonal twist		45.2	42.1

[a] Numbers in parentheses are esd's (derived from the full matrix least-squares refinement) of the last digit.

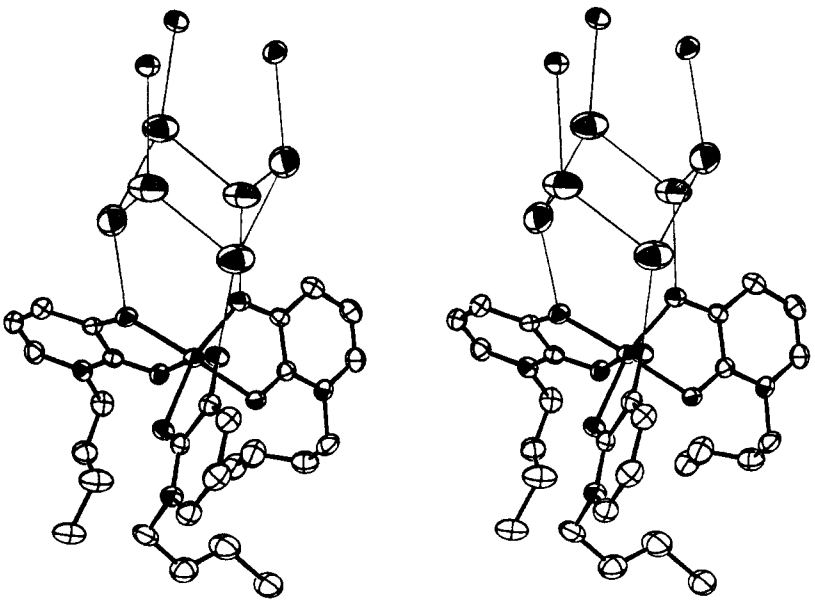

Figure 3. Stereographic projection of $FeL'_3 \cdot 3H_2O$, showing the tris complex of $[L']^-$ with iron, the hydrogen-bonded water oxygens, and, at the top, three O2 atoms from another molecule of the iron complex. Atoms are shown at the 20% probability levels. Partial occupancy atoms C71, C81, and C91 and all hydrogen atoms are omitted. Thin lines are hydrogen bonds (vertical in this view). A 3-fold axis passes through the iron atom and a $\bar{3}$ center lies just above the Fe, interrelating the six H_2O's shown.

Table IV. Occupancies, Positional Parameters, and B_{eq}'s for Tris[*N*-butyl-3-hydroxy-2(1*H*)-pyridinonato]iron(III) Trihydrate ($FeL'_3 \cdot 3H_2O$)[a]

atom	occ	*x*	*y*	*z*	B_{eq},[b] Å^2
Fe	1	0.000	0.000	0.18672 (3)	4.23 (1)
OW	1	0.0362 (2)	0.1490 (2)	0.0343 (1)	10.8 (1)
O1	1	0.1218 (1)	0.0789 (1)	0.23952 (7)	4.57 (4)
O2	1	0.1081 (1)	−0.0127 (1)	0.14604 (6)	4.89 (5)
N	1	0.2812 (1)	0.0996 (2)	0.25886 (9)	4.95 (6)
C1	1	0.1976 (2)	0.0678 (2)	0.2257 (1)	4.32 (7)
C2	1	0.1947 (2)	0.0194 (2)	0.1742 (1)	4.46 (7)
C3	1	0.2783 (2)	0.0109 (2)	0.1592 (1)	5.80 (8)
C	1	0.3641 (2)	0.0489 (2)	0.1945 (1)	6.46 (8)
C5	1	0.3643 (2)	0.0912 (2)	0.2429 (1)	6.03 (8)
C6	1	0.2804 (2)	0.1436 (2)	0.3129 (1)	6.59 (9)
C7	0.75	0.2567 (3)	0.0721 (4)	0.3580 (2)	8.0 (1)
C8	0.75	0.1597 (4)	−0.0211 (4)	0.3574 (2)	9.9 (2)
C9	0.60	0.1440 (5)	−0.1034 (5)	0.4036 (2)	9.0 (2)
C71	0.25	0.1941 (9)	0.0503 (9)	0.3525 (6)	7.0 (3)*
C81	0.25	0.229 (1)	−0.031 (1)	0.3612 (7)	9.2 (4)*
C91	0.40	0.128 (1)	−0.064 (1)	0.4190 (6)	15.3 (5)*

[a] Atom naming is explained in Figure 4; estimated standard deviations of the last digit are given in parentheses. [b] Asterisk indicates a fixed isotropic thermal parameter.

Figure 3 shows a stereoscopic ORTEP[30] projection of the iron complex and the hydrogen-bonding network connecting two molecules of FeL'_3 via six water molecules centered around the point of $\bar{3}$ symmetry. Each iron atom lies on the 3-fold axis so that the three ligands of the complex are symmetry related. The model employed for the disorder in the butyl groups adequately describes the electron density in the hydrophobic region of the molecule, so that the bonding geometry around the iron center is not affected. A search for interligand contacts that might account for the disorder revealed no C–C distances less than 3.6 Å, so that it appears likely that the disorders in each of the three butyl groups of one molecule are substantially independent of each other.

In spite of the relatively short hydrogen bonds linking the water oxygens with each other (2.61 Å) and with O2 (2.74 Å), the thermal parameters of the water oxygens are large (B_{eq} = 10.8 Å^2) and anisotropic (rms vibration: minimum 0.285 Å; maximum 0.462 Å), suggesting slight disorder. No evidence of such disorder was found in Fourier or difference Fourier maps, although the latter show peaks where the water protons would be expected. When these protons were included in the structure model (with B = 11 Å^2), the error indices increased, so in the final model the protons were not included.

Table III compares bond lengths and angles in the free ligand HL′ with those in its ferric complex FeL'_3 and those in tris[3-hydroxy-2(1*H*)-pyridinonato]iron(III)[12] (FeL_3). Like that of FeL'_3, the crystal structure of FeL_3 is rhombohedral with Z = 6 (hexagonal axes) and the iron atom on the 3-fold axis, but in this case the $R\bar{3}c$ symmetry requires 2-fold axes that also pass through the iron atom. To accommodate the 2-fold axes, the 3-hydroxy-2-pyridinonate ligands are disordered into two half-occupancy conformations that are only partially resolved. Thus, bond lengths and angles from FeL_3 are considerably uncertain.[12] In contrast, the hydroxypyridonate portion of FeL'_3 is ordered and the bond lengths and angles are considered accurate and reliable.

The alternating C–C bond lengths in the pyridine ring and the differences in bond lengths involving O1 and O2 indicate that the localized resonance form plays an important role in determining the structure of HL′ and FeL'_3. Upon binding of iron to the ligand, the single and double C–O bond lengths become more similar, indicating that π-delocalization is enhanced by metal chelation.

The formally anionic O2 in FeL'_3 is 0.07 Å closer to Fe than is O1 (the carbonyl oxygen). Figure 4 compares bond lengths for the iron complexes of a variety of bidentate anionic ligands

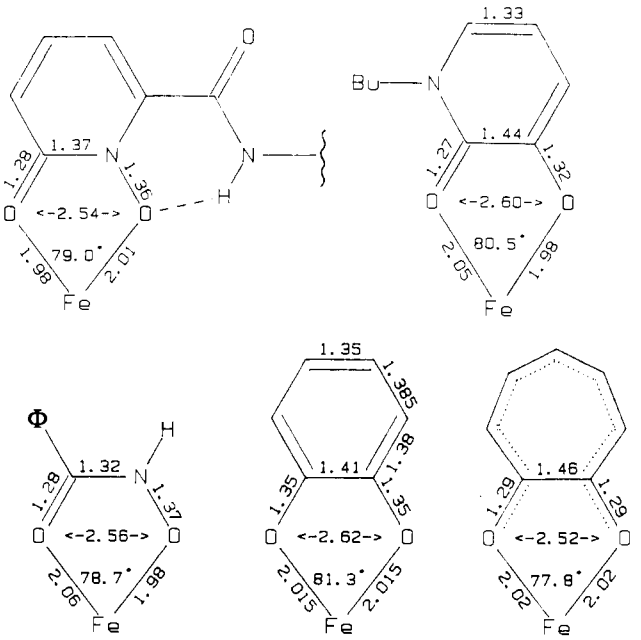

Figure 4. Comparison of chelate ring geometries for tris iron complexes of a 1,2-Hopo derivative (1,5-bis[(1,2-dihydro-1-hydroxy-2-oxopyridin-6-yl)carbonyl]-1,5-diazapentane[19]), a 3,2-Hopo derivative (HL′), benzohydroxamic acid,[32] catechol,[35] and tropolone.[34]

with oxygen donor atoms. All form five-membered chelate rings with high-spin iron(III) with 2.0-Å Fe–O bond distances. The asymmetric Fe–O distances of FeL'_3 resemble those of the 1:3 complex of iron with benzohydroxamic acid,[31,32] a ligand with affinities for protons and iron[33] very close to those of 3,2-Hopo.[12]

Note Added in Proof: The structure of *mer*-tris(3-hydroxy-2-methyl-4(4*H*)-pyranonato)iron(III) has average Fe–O and C–O distances of the formally anionic (3) oxygen (1.99 and 1.33 Å) and carbonyl (4) oxygen (2.06 and 1.26 Å) which are very similar to those of FeL'_3.[38]

The ligand bite distances (O–O) and angles (O–Fe–O) in FeL'_3 and FeL_3 are larger than those in the benzohydroxamate or tropolonate complexes[34] and are on the order of those in the catecholate complex.[31] The relatively large bite distance is attributed to the largely single-bond character of the C1–C2 bond (which is 0.03 Å longer than the C3–C4 bond, also nominally a single bond). This long C–C bond closest to the iron and the short C–C bond on the other side of the ring (C4–C5 is 0.03 Å shorter than C2–C3) are also observed in potassium tris(catecholato)-ferrate(3−) sesquihydrate.[35]

The trigonal twist angle (that is, the ligand O–Fe–O bite angle measured on a 2-dimensional projection perpendicular to the trigonal axis)[31] of FeL'_3 is diminished considerably from the idealized value of 60° for octahedral coordination, as it is for other tris-bidentate complexes of high-spin iron(III). In the case of FeL'_3 this angle is 45.2°, very similar to the 44.7° angle found in potassium tris(catecholato)ferrate(3−) sesquihydrate[35] and somewhat larger than the trigonal twist angle of FeL_3 (42.1°).[12] The trigonal face defined by the O2 (deprotonated hydroxy) atoms has longer sides (O2–O2 distances are 2.97 Å) and is closer to the iron (0.99 Å) than the trigonal face defined by the O1 (carbonyl) oxygens (2.77 and 1.28 Å). This opening of the O2 face (top face in Figure

(30) Johnson, C. K. "ORTEP"; Report ORNL-3794; Oak Ridge National Laboratory: Oak Ridge, TN, 1965.

(31) Raymond, K. N.; Abu-Dari, K. A.; Sofen, S. R. Stereochemistry of Microbial Iron Transport Compounds. In *Stereochemistry of Optically Active Transition Metal Compounds*; Douglas, B. E., Saito, Y., Eds.; ACS Symposium Series 119; American Chemical Society: Washington, DC, 1980; pp 133–167.

(32) Linder, J. J.; Goettlicher, S. *Acta Crystallogr., Sect. B* **1969**, *B25*, 832–842.

(33) Martell, A. E.; Smith, R. M. *Critical Stability Constants*; Plenum: New York, 1974–81; Vols. 1–5.

(34) Hamor, T. A.; Watkin, D. J. *J. Chem. Soc., Chem. Commun.* **1969**, 440.

(35) Raymond, K. N.; Isied, S. S.; Brown, L. D.; Fronczek, F. R.; Nibert, J. H. *J. Am. Chem. Soc.* **1976**, *98*, 1767–1774.

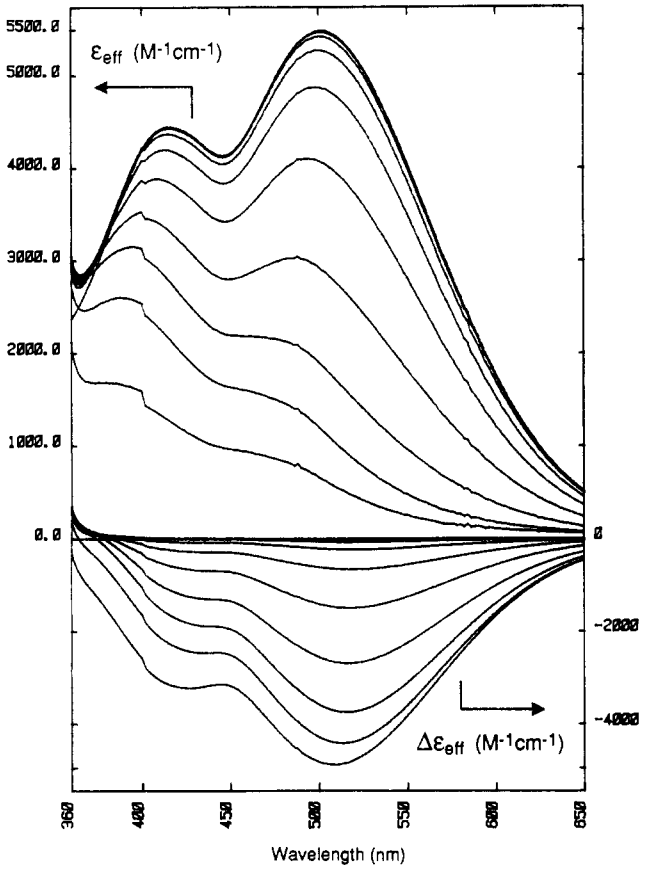

Figure 5. Spectral changes observed when a solution originally 37 μM in iron(III), 3.2 mM in HL′, and 0.1 M in KNO_3 is titrated with 0.10 M KOH at 25 °C in a 1.0 cm path length cell. The absorbance data have been converted to effective extinction coefficients ($\epsilon_{eff} = A/[\text{path length} \times C_{Fe}]$) to correct for the effects of dilution. In order to compensate for detector base-line drift, the average of absorbance values between 790 and 800 nm was subtracted from each spectrum. The spectral glitch at 400 nm is due to differential drift in the UV and visible detectors of the spectrophotometer. The ϵ_{eff} throughout the visible region decreases with increasing p[H]. The p[H] values for the plotted spectra are, from bottom to top, 12.08, 11.82, 11.58, 11.34, 11.11, 10.88, 10.63, 10.38, 10.12, and 7.34. The last two spectra are indistinguishable and are only slightly higher than the p[H] 10.38 spectrum. The $\Delta\epsilon_{eff}$ plot is shown at the bottom, where the ϵ_{eff} spectrum at p[H] 7.34 is subtracted from each plotted spectrum.

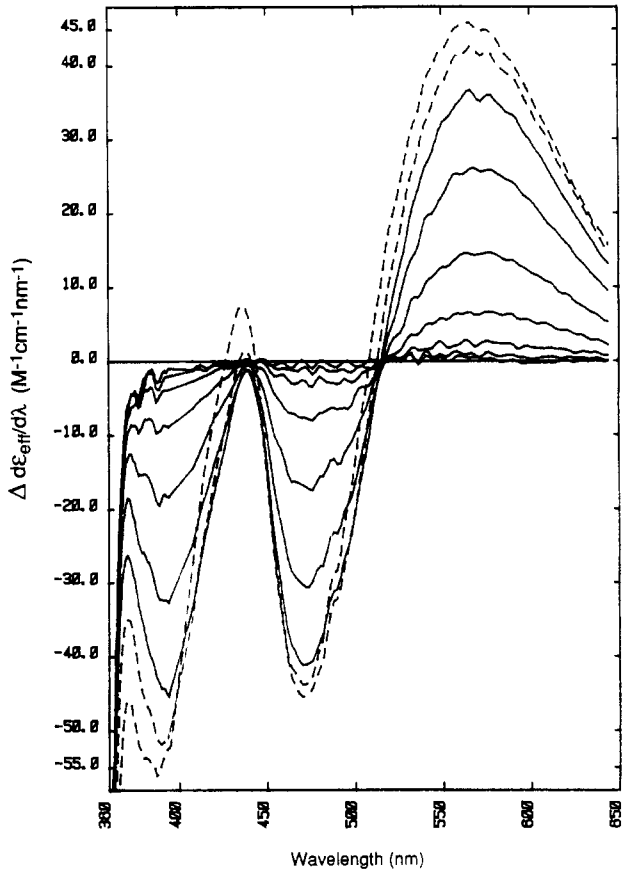

Figure 6. First-derivative plot of the difference spectra shown in the bottom half of Figure 5. This plot was generated by dividing the $d(A)/d\lambda$ spectra by C_{Fe} and subtracting from each the $d(\epsilon_{eff})/d\lambda$ spectrum for p[H] 7.34. To aid visualization, the data were subjected to a smoothing algorithm and linear interpolation was used between 392 and 408 nm to remove the effects of the differential detector drift referred to in the caption for Figure 5. The derivative spectra correspond to the same p[H] values as in Figure 5; those for p[H] 11.82 and 12.08 have been dashed to emphasize their deviation from the isosbestic behavior observed for the other spectra at 516 nm.

3) can be explained by the repulsion between negative charges present on the O2 atoms, as opposed to the lesser repulsion between the formally neutral carbonyl oxygen atoms.

Solution Equilibria. As expected, the basicity of 3,2-Hopo (log K_a = 8.66[12]) is increased slightly by the substitution of an alkyl group at the nitrogen. The value determined by potentiometric titration for the *N*-butyl derivative HL′ is log K_a = 9.06.

The complexation of iron by excess HL′ was investigated by spectrophotometric titration of a solution 37 μM in iron(III) and 2.9 mM in HL′. The solution p[H] was varied between 2.3 and 12.2. Between p[H] 2.4 and 7, the spectra changed with an isosbestic point at 565 nm (data not shown) and were very similar to those of solutions of iron and excess 3,2-Hopo in the same p[H] range.[12] Thus we assign these spectral changes to

$$[FeL'_2]^+ + HL' = FeL'_3 + H^+$$

on the basis of previous work with 3,2-Hopo.

Between p[H] 7 and 10 no visible spectral changes were noted in the Fe(III)/HL′ titration. The spectral changes above p[H] 10 are shown in absorbance and derivative ($dA/d\lambda$) forms in Figures 5 and 6. The latter shows isosbestic points over the p[H] range 10.0–11.5, suggesting only two colored species are at equilibrium in this p[H] range. The identity of the high-p[H] form will be discussed further below. Above p[H] 11.5 the derivative spectra (Figure 6) show deviations from the isosbestic points, indicating additional species were formed. At the highest p[H] values spectral changes after addition of base became slow, slight turbidity was evident, and the observed spectral changes exhibited hysteresis upon reacidification. These properties suggest the loss of color (Figure 5) above p[H] 11.5 is due to formation of hydrated ferric oxides.

The spectra between p[H] 2.4 and 11.3 were expressed as sums of three orthogonal components (n_c = 3; see Experimental Section) with noise level $||R||$ (=0.0001), suggesting the existence of only three colored species in accord with the two p[H] ranges exhibiting isosbestic behavior. The component spectra are shown in Figure S1.[29] Least-squares fits of the componentized data (Figure 7) indicate the equilibrium occurring above p[H] 10 has a two-proton stoichiometry with an apparent log K_{a1} + log K_{a2} = 22.6. On the basis of the low magnitude of its refined extinction spectrum (Figure 7), the species formed appears to be a mono(hydroxypyridonate) complex, as indicated in Scheme II, which also shows refined equilibrium constants and values of λ_{max} for the various species, as determined by a least-squares fit. Fifty spectra for solutions between p[H] 2.4 and 11.3 were fit. The root-mean-square deviation between observed and calculated spectra was 0.000 45 (Figure S2).[29] For comparison, the root-mean-square absorbance of the data set equals 0.138.

The stepwise formation constant (log K_3) for $[FeL'_2]^- + [L']^- \rightleftarrows FeL'_3$ is larger by 0.6 than the value for the formation of FeL_3,[12] indicating that the Lewis basicity of 3,2-Hopo toward iron is increased by electron donation from the *N*-alkyl group. Since the *N*-butyl group increases the protonation constant (log K_a) by a similar amount, the net effect of the *N*-butyl group on iron complexation ability is minor below p[H] 8, because deprotonation

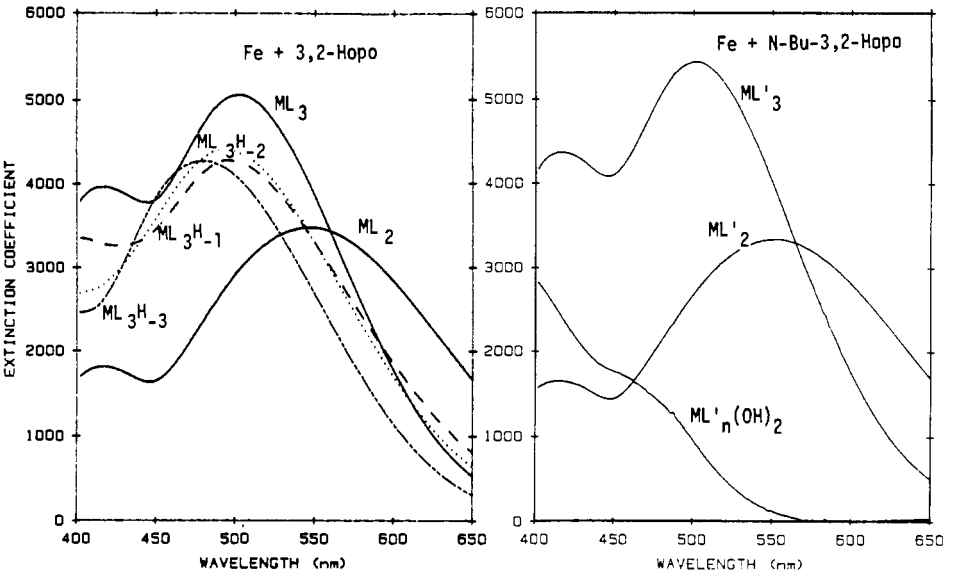

Figure 7. Refined extinction coefficient spectra for iron-containing species found in titration of iron/3,2-Hopo and iron/HL′ solutions.

Scheme II

HL′ = N-butyl-3-hydroxy-2(1H)-pyridinone

$FeL'_2^+ + L'^- \rightleftharpoons FeL'_3 \quad (\log K = 8.7)$

$FeL'_3 \overset{-2\,L'^- \,-2\,H^+}{\rightleftharpoons} FeL'(OH)_2 \quad (\log K = -25.1)$

$FeL'(OH)_2 \overset{-\,H^+}{\longrightarrow} Fe(OH)_3 + L'^- \quad (pH > 11.5)$

553 & 414nm, ε = 3280 & 1550 | 501 & 416 nm, ε = 5440 & 4370 | sh 451 nm, ε = 1740 | turbidity

HL = 3-hydroxy-2(1H)-pyridinone (3,2-Hopo)

$FeL_2^+ + L^- \rightleftharpoons FeL_3 \quad (\log K = 8.1)$

$FeL_3 \overset{-\,H^+}{\rightleftharpoons} FeL_2(H_{-1}L)^- \quad (\log K_a = 9.2)$

$FeL_2(H_{-1}L)^- \overset{-\,H^+}{\rightleftharpoons} FeL(H_{-1}L)_2^{2-} \quad (\log K_a = 10.5)$

$FeL(H_{-1}L)_2^{2-} \overset{-\,H^+}{\rightleftharpoons} Fe(H_{-1}L)_3^{3-} \quad (\log K_a = 12.0)$

548 & 415 nm, ε = 3690 & 1880 | 502 & 417nm, ε = 5060 & 3970 | 497 nm, ε = 4320 | 494 nm, ε = 4370 | 476 nm, ε = 4480

of the hydroxypyridinone ligand must occur before it binds to the ferric ion.

The stability of the 3:1 complex of HL′ with iron(III) up to p[H] 10 (at 3 mM HL′) contrasts with the deprotonation of the corresponding complex of 3,2-Hopo with a log K_a of 9.[12] The absence of this p[H] 9 deprotonation in FeL'_3 suggests this process is due to the loss of the proton from the nitrogen atom of one ligand in FeL_3. Similar deprotonations are observed at pH 9–10 in copper and zinc complexes of 3,2-Hopo and of its isomer 3-hydroxy-4-(1*H*)-pyridinone.[14]

In our earlier spectrophotometric titration study of iron complexation by 3,2-Hopo, we noted ligand concentration dependence of equilibria at p[H] 10–11 in the presence of excess 3,2-Hopo, which suggested loss of ligand. This result, based on two titrations, is difficult to reconcile with the relatively constant magnitude of the visible absorbance peak as it was blue-shifted between p[H] 8 and 11. The extinction coefficient at λ_{max} (ϵ = 4500 M^{-1} cm^{-1}) is typical for ligand-to-metal charge-transfer complexes of 3:1 (catecholato)- or (hydroxypyridonato)iron complexes.[12] Furthermore, the hydrolysis of FeL'_3 at p[H] 11 causes a major loss in visible absorbance. Thus, we have reinvestigated the deprotonation reactions of FeL_3 above p[H] 7 by performing a series of six spectrophotometric titrations. These titrations differed from the earlier two titrations in that the pH electrodes were calibrated more accurately for the basic p[H] range (by using freshly prepared dilute KOH rather than NBS buffer solutions). In addition, the p[H] range between 11 and 12 was included in the new titrations, revealing an additional equilibrium not noted before (see below). Titrations were performed in both p[H] directions to check for hysteresis.

Figure 8 shows absorbance changes observed as the p[H] of FeL_3 solution is raised from 7 to 12. Isosbestic points at 593 and 390 nm were observed from p[H] 7 to 9.5, strongly suggesting that FeL_3 and one other colored species are the only iron-containing species in solution in this p[H] range.[36] Around p[H] 10.5 approximate isosbestic points occur at 436 and 498 nm, but this isosbestic behavior disappears above p[H] 11.4. This suggests at least two additional iron-containing species exist above p[H] 9.5.

The existence of four colored species between p[H] 7 and 12 is supported by the spectral componentization (Figure S3[29]), which indicates $n_c = 4$. (Table V shows that attempts to use $n_c = 3$ result in $||R||$ values an order of magnitude larger than for $n_c = 4$, whereas use of $n_c = 5$ decreases $||R||$ by only 10%, with the exception of the titration employing the largest C_L. In this case ligand absorbance changes are significant compared with noise, and they add an additional component.) The least-squares fits to the data (as shown in Figure S4[29]) indicate two one-proton deprotonations occur between p[H] 8 and 11 and that these equilibria do not involve loss of ligand, since the observed values of log K_a do not vary significantly over the 4-fold range in C_L used in titrations. Average values for equilibrium constants and ex-

(36) The solid lines in Figure 7 are slightly nonisosbestic at 390 nm because of small changes in ligand absorbance and because of differential drift of the UV and visible detectors (which causes the glitch at 400 nm).

Table V. Details of Spectral Componentization of and Refinement on Spectral Titration Data[a]

	3,2-Hopo						3
C_{Fe}, μM (av)[b]	34.8	16	19	19	33.2	9.3	37
C_L, mM (av)[b]	10.5	4.7	12	2.9	2.8	2.9	2.9
titrant	12 M HCl	0.1 M KOH	0.1 M KOH	0.1 M KOH	12 M HCl	0.1 M HCl	0.1 M KOH
p[H] range	11.5–7.0	7.4–11.9	7.1–11.5	7.0–11.5	11.5–7.1	7.0–11.5	2.4–11.3
no. of spectra	30	32	30	35	22	50	50
			Componentization				
$\|\|R\|\|$ (n_c = 3)[c]	0.003 01	0.002 11	0.001 38	0.001 61	0.002 92	0.000 79	0.000 09
$\|\|R\|\|$ (n_c = 4)	0.000 64	0.000 17	0.000 34	0.000 17	0.000 50	0.000 084	0.000 06
$\|\|R\|\|$ (n_c = 5)	0.000 59	0.000 16	0.000 16	0.000 15	0.000 46	0.000 076	0.000 04
			Refinement				
log K_{a1}	9.21 ± 0.01	9.21 ± 0.01	9.17 ± 0.01	9.17 ± 0.01	9.18 ± 0.01	9.24 ± 0.01	
log K_{a2}	10.46 ± 0.02	10.57 ± 0.03	10.57 ± 0.06	10.59 ± 0.01	10.52 ± 0.02	10.54 ± 0.02	22.55 ± 0.02[d]
log K_{a3}	11.73 ± 0.06	11.98 ± 0.05	12.01 ± 0.27	12.16 ± 0.07	12.15 ± 0.13	12.2[e]	8.76 ± 0.01[f]
$\lambda_{max}(FeL_3)$[g]	416 (3950)	416 (3920)	416 (3900)	417 (3990)	417 (4000)	418 (4050)	416 (4370)
	502 (5030)	502 (5010)	504 (5000)	502 (5091)	502 (5070)	502 (5170)	501 (5440)
$\lambda_{max}([FeL_3H_{-1}]^-)$	500 (4330)	496 (4280)	496 (4280)	497 (4360)	496 (4260)	496 (4440)	
$\lambda_{max}([FeL_3H_{-2}]^{2-})$	494 (4380)	492 (4360)	495 (4300)	492 (4410)	494 (4260)	496 (4500)	451 sh (1950)
$\lambda_{max}([FeL_3H_{-3}]^{3-})$	482 (4620)	476 (4480)	478 (4760)	472 (4100)	468 (4060)	464 (4360)	
$\|\|R\|\|$[h]	0.000 98	0.000 61	0.000 88	0.000 36	0.000 77	0.000 29	0.000 45

[a] Absorbance values used in the componentization and subsequent refinement were from 402 to 650 nm (125 array elements on the visible detector of the spectrometer) and were base-line corrected by subtracting the average absorbance (790–800 nm). [b] Concentrations vary due to dilution by titrant. [c] $||R||$ is defined by eq 1. [d] The value of 22.55 corresponds to log K_{a1} + log K_{a2}; i.e., the log K for $[FeL'_n(OH)_2]^{1-n} + 2H^+ + (3-n)[L']^- = FeL'_3$, where n = 3. If one assumes n = 1 or 2, then the refined log K is 27.63 or 25.09, respectively. The refined ϵ spectrum of $[FeL_nH_{-2}]^{1-n}$ is virtually independent of n. [e] Value of log K_{a3} fixed. When this restraint is removed, log K_{a3} increases indefinitely and $\epsilon([FeL_3H_{-3}]^{3-})$ also diverges (and becomes negative for $\lambda > 600$ nm). [f] log K_3 (for $[FeL'_2]^+ + [L']^- = FeL'_3$). [g] Refined extinction coefficients (M^{-1} cm^{-1}) at λ_{max} (nm) are given in parentheses. [h] $||R||$ is defined by eq 1, but with A_{calc} calculated from refined equilibrium constants and extinction coefficients.

tinction coefficients are given in Scheme II.

The data above p[H] 11 were poorly fit unless another one- or two-proton dissociation was added to the model. However, the refined values for these constants indicate this deprotonation to be less than half complete when the titrations were stopped at p[H] near 11.5 (above this p[H] turbidity and loss of color have been observed due to formation of ferric hydroxide). For most titrations, the data were fit somewhat better by a one-proton step. The refined log K_{a3} values generally decrease with increasing ligand concentration, which is probably coincidental, since a ligand dissociation process would be expected to give the opposite trend. The refined extinction coefficients of the highest p[H] species vary from titration to titration and are highly correlated with the refined values of log K_{a3} due to the small amount of $[ML_3]^{3-}$ formed. The most accurate values for log K_{a3} and ϵ of $[ML_3]^{3-}$ are expected to be derived from the titration shown in Figure 8, which was extended to p[H] 11.9, and these are reported in Scheme II.

Visible Absorption Spectra. The refined extinction coefficients for the species shown in Scheme II are shown in Figure 7. The visible extinction coefficients exceeding 1000 M^{-1} cm^{-1} are indicative of ligand-to-metal charge-transfer (LMCT) transitions. The LMCT intensity is proportional to the number of ligands; for hydroxypyridinonate and catecholate ligands, the transition intensity is about 1500 M^{-1} cm^{-1} per bound ligand.[12] In addition, the LMCT bands increase in energy with the crystal field strength of the overall ligand set, presumably due to the raising of the energy of the half-filled iron d orbitals.[37] The progression of λ_{max} from 600 to 550 to 500 nm for the 1:1, 2:1, and 3:1 complexes of both HL′ and HL with iron indicates that the hydroxypyridinone ligands generate a greater crystal field than the water they replace. The near-identity of the λ_{max} values for the two sets of complexes indicates that the energy of the hydroxypyridinone π orbital responsible for the LMCT is unaffected by the *N*-butyl substituent.

The magnitude of the extinction coefficient was used in the assignment of the first hydrolysis product of FeL'_3 as $FeL'(OH)_2$. The blue shift of the hydrolysis product (Figure 7) indicates the crystal field strength of the hydroxide ligands is stronger than that

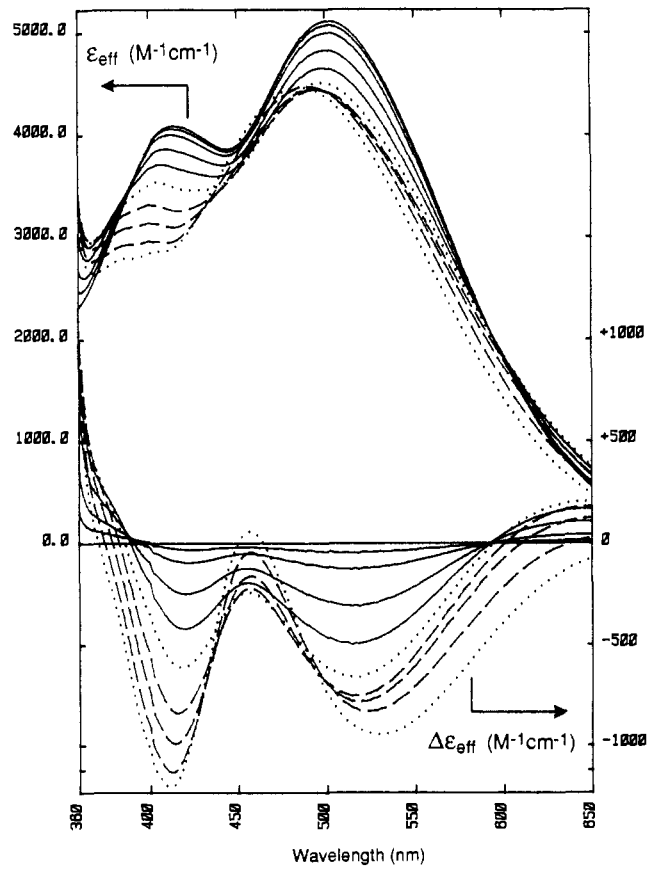

Figure 8. Spectral changes observed when a solution originally 17 μM in iron(III), 5 nM in 3,2-Hopo, and 0.1 M in KCl is titrated with 0.10 M KOH at 25 °C in a 10 cm path length cell. The absorbance data were base-line corrected and converted to ϵ_{eff}, as explained in the caption for Figure 5. The ϵ_{eff} at 410 and 525 nm decreases with increasing p[H]. The p[H] values for the plotted spectra are as follows: (—) 7.39, 8.05, 8.50, 9.01, 9.43; (···) 9.89; (---) 10.44, 10.87, 11.40; (···) 11.87. The spectral changes are more easily visualized from the $\Delta\epsilon_{eff}$ plot shown at the bottom, where the ϵ_{eff} spectrum at p[H] 7.39 is subtracted from each plotted spectrum. In the comparison of Figures 5 and 8, note that the scales of the $\Delta\epsilon_{eff}$ plots differ by a factor of 4.

(37) Pyrz, J. W.; Roe, A. L.; Stern, L. J.; Que, L., Jr. *J. Am. Chem. Soc.* **1985**, *107*, 614–620.
(38) Ahmet, M. T.; Frampton, C. S.; Silver, J. *J. Chem. Soc., Dalton Trans.* **1988**, 1159–1163.

of the ligands of $[L']^-$ they replace. The crystal field strength of the 3,2-Hopo ligand is expected to increase upon N-deprotonation due to the increased negative charge on the ligand, and indeed, blue shifts are observed upon successive deprotonations of FeL_3. However, deprotonation is also expected to raise the ligand orbital energies, and this offsetting effect may account for the small size of the observed blue shift.

Summary. A general and efficient synthetic route to *N*-alkyl-3-hydroxy-2(1*H*)-pyridinone ligands has been devised. The solid-state and neutral and acidic pH solution chemistry of these ligands is similar to that of the N-unsubstituted ligand, 3,2-Hopo. However, in basic solution, the complexes of 3,2-Hopo derive added stability by deprotonating at the ring nitrogen of each ligand, an option unavailable to the N-substituted molecules such as FeL'_3.

Acknowledgment. Walter Kwan assisted with the development of some of the synthetic methods described in this paper. Dr. Larry Loomis helped design and program the automatic spectrophotometric titrator. The crystal structures were performed at the CHEXRAY Diffraction Facility (supported in part by grants from the National Science Foundation), directed by Dr. Fred Hollander. This research was supported by NIH Grant AM32999.

Registry No. **1**, 39658-49-6; **2**, 116407-51-3; **3**, 116407-52-4; **4**, 116407-53-5; 3,2-Hopo, 16867-04-2; 2,5-dimethoxy-2,5-dihydrofuran-2-carboxylic acid methyl ester, 62435-72-7; *n*-butylamine, 109-73-9.

Supplementary Material Available: Tables S1 and S4 (general temperature factor expressions for **3** and **4**), Table S2 (fixed positional parameters and thermal parameters for hydrogen atoms in **3**), Table S5 (fixed positional and thermal parameters and occupancy factors for hydrogen atoms in **4**), Figure S1 (orthogonal component spectra for titrations of ferric ion with HL'), Figure S2 (results from least-squares fit to data of spectral titrations of Fe^{3+} and HL'), Figure S3 (orthogonal component spectra for titrations of Fe^{3+} and L), and Figure S4 (results from least-squares fits to spectral data from titrations of ferric ion with HL) (8 pages); Tables S3 and S6 (observed and calculated structure factors for **3** and **4**) (23 pages). Ordering information is given on any current masthead page.

Contribution from the Dipartimento di Chimica and Dipartimento di Scienza della Terra, Sezione Cristallografia, Università di Perugia, 06100 Perugia, Italy

Out-of-Plane Coordination and Exchange Coupling in Oxygen-Bridged Copper(II) Dimers[1]

B. Chiari, O. Piovesana,* T. Tarantelli, and P. F. Zanazzi

Received January 11, 1988

The syntheses, crystal and molecular structures, and magnetic properties are reported for the new compounds $Cu_2L_2(CH_3COO)_2\cdot 2C_2H_5OH$ (compound E) and $Cu_2L_2(CH_3COO)_2\cdot 2CH_3OH$ (compound M), where L^- is the ligand

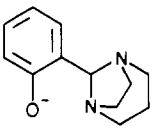

Compounds E and M, which are isostructural, crystallize in the monolinic space group $P2_1/a$, $Z = 2$. Cell dimensions are as follows. Compound E ($Cu_2C_{32}H_{48}N_4O_8$): $a = 20.867$ (3), $b = 10.168$ (3), $c = 7.960$ (3) Å; $\beta = 94.12$ (2)°. Compound M ($Cu_2C_{30}H_{44}N_4O_8$): $a = 20.627$ (3), $b = 9.987$ (3), $c = 7.839$ (3) Å; $\beta = 92.41$ (2)°. The structures were solved by Patterson and Fourier methods and refined to an *R*(unweighted) value of 0.047 for E and 0.041 for M. The two complexes consist of centrosymmetric dimeric units that are well separated from one another. The binuclear structures are held together by phenoxo bridges between the copper atoms. The Cu–O(bridging) separations average 1.97 Å. The bridging CuOCu angles in E and M are 101.6 (4) and 102.4 (1)°, respectively. The geometry around the copper atoms may be described as distorted square-pyramidal. The apical, weak bond involves the oxygen atom of the solvent molecule and is stronger in E, 2.267 (4) Å, than in M, 2.370 (4) Å. The base of the coordination pyramid deviates from planarity, and the distortion may be approximately described as being toward tetrahedral geometry. The dihedral angle, τ, between the bridging plane and the plane of the remaining ligands is 14° in both compounds. The two dimers exhibit antiferromagnetic exchange interactions with singlet–triplet splittings of 364 cm^{-1} for E and 420 cm^{-1} for M. A comparison of the structural and magnetic data obtained for the present compounds with corresponding data for previously characterized planar and nonpolar compounds involving similarly bridged Cu_2O_2 moieties indicates that the apical ligands have a definite role in the magnetic coupling in E and M. A general discussion of the magnetic consequences that may be expected when the coordination environment at copper changes from 4 to (4 + 1) is also given.

Introduction

Doubly bridged copper(II) dimers involving a Cu_2O_2 moiety, owing to the rather unique variety of structural types and spin–spin interactions that characterize their crystal chemistry, have provided a rich opportunity for the investigation of structural effects on magnetic coupling.[2]

Hatfield et al.[2a,b,3] have demonstrated that, in planar hydroxo-bridged dimers of type I, the singlet–triplet splitting resulting from exchange coupling, $-2J$, is a linear function of the bridging CuOCu angle, ϕ, according to eq 1. A quite different structural dependence of the magnetic properties has been observed by Sinn et al.[4] for a series of diphenoxo-bridged dimers of type II, in which the ligand environment is considerably distorted from planar toward tetrahedral geometry. These compounds conform to eq

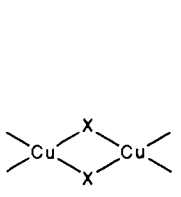

I

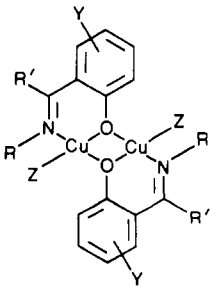

II

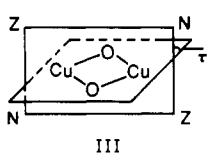

III

2,[1c] where τ is the dihedral angle between the plane of the Cu_2O_2 bridging unit and the plane of the remaining ligands, III.

$$2J\ (cm^{-1}) = -74.53\phi + 7270 \quad (1)$$

$$2J\ (cm^{-1}) = 29.7\tau - 1473 \quad (2)$$

* To whom correspondence should be addressed at the Dipartimento di Chimica.

 © 1988 American Chemical Society